New oxygen hole centres in the x-ray storage phosphor BaFBr

1999 J. Phys.: Condens. Matter 11 1723

(http://iopscience.iop.org/0953-8984/11/7/006)

J. Phys.: Condens. Matter **11** (1999) 1723–1733. Printed in the UK PII: S0953-8984(99)97746-9

New oxygen hole centres in the x-ray storage phosphor BaFBr

S Schweizer and J-M Spaeth

Universität-GH Paderborn, Warburger Strasse 100A, D-33098 Paderborn, Germany

Received 22 September 1998

Abstract. After room temperature x-irradiation of BaFBr single crystals grown from a stoichiometric mixture of BaF_2 and $BaBr_2$ two new oxygen hole centres were discovered and investigated by electron paramagnetic resonance (EPR) and electron nuclear double resonance (ENDOR). One is an oxygen ion (O^-) on a bromide site, however, with different superhyperfine (shf) interactions compared to the one investigated previously. The other one is an oxygen molecule (O_2^{3-}) with one oxygen on a fluoride site and one on the neighbouring bromide site, both sharing one hole. In total, now four different paramagnetic oxygen hole centres are known in stoichiometric BaFBr single crystals. Moreover, some shf interaction parameters of the F(F^-) centre were determined.

1. Introduction

BaFBr single crystals grown from the melt of a stoichiometric mixture of BaF_2 and $BaBr_2$ with the Bridgman method are normally contaminated with oxygen which is incorporated as O^{2-} on a bromide or a fluoride site. This contamination is practically unavoidable [1–3]. Upon x-irradiation at room temperature the incorporated O^{2-} ions capture holes to form paramagnetic O^- hole centres. The structure of two oxygen hole centres was determined with electron paramagnetic resonance (EPR) and electron nuclear double resonance (ENDOR) spectroscopy. In one centre O^- occupies a F^- site (centre [1, 2]), in the other a Br^- site (O_{Br}^- centre [4]).

One role of the oxygen contamination in the x-ray storage phosphor BaFBr:Eu^{2+} is certainly that O^{2-} capture holes. It was shown previously that it is unlikely that these hole centres are the active hole centres in the photostimulated luminescence (PSL) process since bleaching into the F centre bands can only partly destroy the O^- hole centres while the number of F centres can be decreased to practically zero. On the other hand, the investigation of the F centre production as a function of the oxygen content showed that oxygen clearly enhances the F centre production [3], which was understood since the incorporation of O^{2-} on a halide site in the matlockite BaFBr structure introduces halide vacancies because of charge compensation. These vacancies facilitate the formation of F centres upon x-irradiation.

In this paper we report two additional paramagnetic oxygen centres which were discovered in the EPR spectrum at a different temperature than used previously to investigate the O_{Br}^- and O_F^- centres. Another O_{Br}^- centre with different superhyperfine (shf) interactions than that of the previously investigated centre and a molecular ion O_2^{3-} were discovered. Their structures are determined using EPR and ENDOR.

0953-8984/99/071723+11$19.50

2. Experiment

2.1. Sample preparation

BaFBr single crystals were grown in graphite crucibles with the Bridgman method from a stoichiometric mixture of BaF_2 and $BaBr_2$ under an argon atmosphere. The ^{17}O doped BaFBr single crystals were grown with an additional doping of anhydrous BaO which was enriched with approximately 35% of the magnetic isotope ^{17}O. The samples were cut with a wire saw. Because of the matlockite structure of BaFBr the crystals could be cleaved perpendicular to the *c*-axis. The samples could be oriented for a rotation of the magnetic field from parallel to the *c*-axis into the *ab*-plane and within the *ab*-plane. Prior to EPR and ENDOR investigations the crystals were x-irradiated for about 4 hours at room temperature (tungsten anode, 50 kV, 30 mA). After x-irradiation the crystals were coloured dark blue. The measurements were performed with a computer-controlled custom-built EPR/ENDOR spectrometer.

3. Experimental results

3.1. EPR measurements on x-irradiated BaFBr single crystals

After x-irradiation of BaFBr at room temperature the two oxygen hole centres O^-_{Br} [4] and O^-_F [1, 2] investigated previously dominate the EPR spectra for $T < 30$ K. They superimpose two hitherto unknown centres which are only clearly visible by EPR for $T > 50$ K. Figure 1 shows the EPR angular dependences of these two new centres which are labelled with $(O^-_{Br})^*$ and $(O_F–O_{Br})^{3-}$, respectively (see below for their identification). The $(O^-_{Br})^*$ and the $(O_F–O_{Br})^{3-}$ centres have single, symmetric EPR lines without resolved hyperfine (hf) or shf structure. The EPR angular dependence of the $(O^-_{Br})^*$ centre can be described by an axial *g*-tensor with the parallel component parallel to the *c*-axis. The $(O_F–O_{Br})^{3-}$ centre shows site splitting; the defect symmetry is lower than that of the $(O^-_{Br})^*$ centre. The analysis yields a monoclinic symmetry. The *g*-values of these two new centres as well as the published data for the $F(Br^-)$, the $F(F^-)$, the O^-_{Br} and the O^-_F centre are listed in table 1.

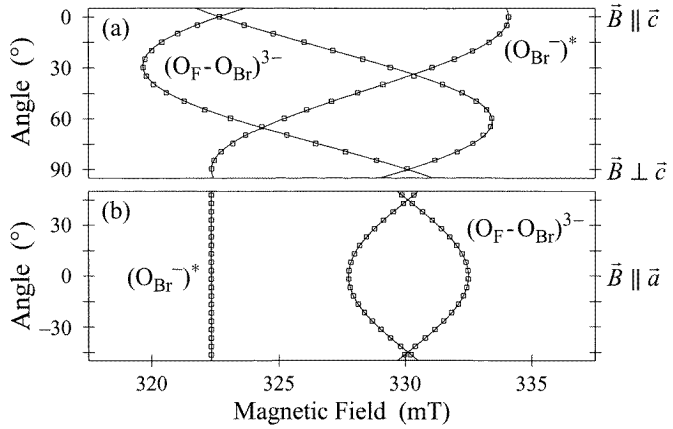

Figure 1. EPR angular dependence of the $(O^-_{Br})^*$ and the $(O_F–O_{Br})^{3-}$ centre in BaFBr for a rotation of the magnetic field (a) from the *c*-axis into the *ab*-plane and (b) within the *ab*-plane, measured at $T = 80$ K ($\nu = 9.335$ GHz). The open squares represent the experimental line positions; the solid lines are calculated by using the *g*-tensors of table 1.

Table 1. g-values of the $(O^-_{Br})^*$ and the $(O_F–O_{Br})^{3-}$ centre as well as the published g-values for the $F(Br^-)$, the $F(F^-)$, the O^-_{Br} and the O^-_F centres in BaFBr. The angle ϑ is measured with respect to the c-axis in the ac- (bc-) plane.

Centre	g_{xx}	g_{yy}	g_{zz}	ϑ (°)	Literature
$(O^-_{Br})^*$	2.069		1.996	—	this work
$(O_F–O_{Br})^{3-}$	2.006	2.104	1.997	54	this work
$F(Br^-)$	1.99		1.98	—	[5]
$F(F^-)$	—		2.00	—	[5]
O^-_{Br}	2.2481		1.9781	—	[4]
O^-_F	2.0419		2.0202	—	[1, 2]

For an axial symmetry about the c-axis three different sites are possible: a bromide site, a fluoride site or an interstitial site, in which the defect can be shifted along the c-axis. Since the EPR line shows no resolved shf structure, further structural information can only be gained from ENDOR investigations.

The site splitting of the $(O_F–O_{Br})^{3-}$ centre indicates that it is not on a highly symmetric site but has a more complex character with several centre orientations in the lattice. Four different centre orientations were found. They cannot be seen, however, in the angular dependences of figure 1 because there are two pairs of two magnetically equivalent centre orientations. The complex is orientated in the ac- (bc-) plane with an angle ϑ of 54° between the z-axis of the g-tensor and the crystal c-axis.

3.2. EPR measurements on x-irradiated ^{17}O doped BaFBr single crystals

The EPR spectrum of an ^{17}O-doped BaFBr single crystal (figure 2) shows many more lines than that of the undoped BaFBr single crystal after x-irradiation. The line group placed symmetrically around the central line of the $(O^-_{Br})^*$ centre consists of six equally spaced and

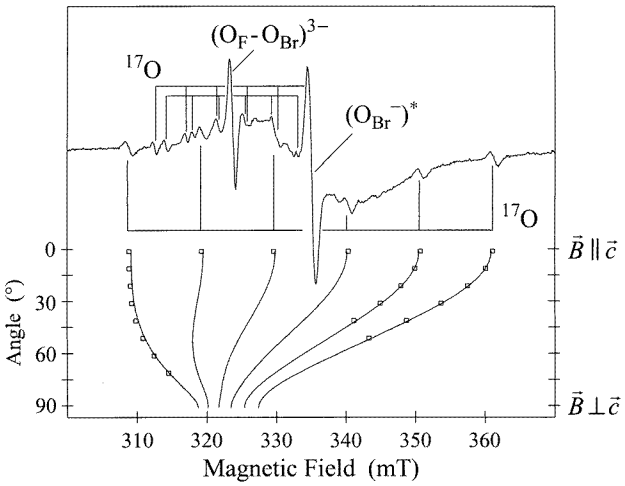

Figure 2. EPR spectrum of the $(O^-_{Br})^*$ and the $(O_F–O_{Br})^{3-}$ centre in ^{17}O-doped BaFBr, measured for $\vec{B} \parallel \vec{c}$ at $T = 65$ K ($\nu = 9.362$ GHz). The bars indicate the ^{17}O hyperfine splittings of the two centres. The ^{17}O hyperfine interaction parameters are listed in table 2.

equally intense lines. These resonances are caused by a hyperfine interaction of the $(O^-_{Br})^*$ centre with the ^{17}O isotope which has a nuclear spin of $5/2$. The symmetry of the ^{17}O interaction tensor is, as is that of the g-tensor, axial. The ^{17}O hf parameters of the $(O^-_{Br})^*$ centre a and b are related to the principal values of the axial hf tensor by

$$A_\perp = a - b \qquad \text{and} \qquad A_\parallel = a + 2b. \tag{1}$$

The angular dependence is shown in figure 2. It is seen that only some of the ^{17}O hf lines were detected. For an orientation of the magnetic field perpendicular to the c-axis the ^{17}O hf lines are very close to each other. The ^{17}O hf data are listed in table 2 (partly determined from ENDOR).

Table 2. ^{17}O hf and quadrupole parameters of the $(O^-_{Br})^*$ and the $(O_F–O_{Br})^{3-}$ centre in BaFBr. The subscripts 1 and 2 represent the two different sites of the ^{17}O nuclei.

Centre	a/h (MHz)	b/h (MHz)	q/h (MHz)
$(^{17}O^-_{Br})^*$	63.9	114.0	0.41
$(^{17}O_F–^{17}O_{Br})^{3-}$	$\lvert A_1\rvert \parallel \vec{c} \approx 130$		—
	$\lvert A_2\rvert \parallel \vec{c} \approx 110$		—

To find out whether the ^{17}O hf interaction of the $(O^-_{Br})^*$ centre is caused by an interaction with a single oxygen ion or with an oxygen molecule (see e.g. $(O^-_2)_{Cl}$ centre in BaFCl [4]), the ratio between the ^{16}O central line and one ^{17}O hf line was determined. It was found to be about 11:1, as expected for a centre with a single oxygen ion on a site with axial symmetry. EPR lines due to ^{17}O–^{17}O pairs were not observed.

The additional EPR lines of the $(O_F–O_{Br})^{3-}$ centre are also due to ^{17}O hf interactions. In contrast to the $(O^-_{Br})^*$ centre two ^{17}O hf line groups having slightly different hf interactions were observed. The ratio between the ^{16}O central line and one of the ^{17}O hf lines is again about 11:1. This means that the $(O_F–O_{Br})^{3-}$ centre consists of two oxygen ions which are not magnetically equivalent for an orientation of the magnetic field parallel to the c-axis. The two oxygens are placed on different lattice sites. The angle ϑ of 54° between the z-axis of the g-tensor and the c-axis and the fact that the molecule is in the ac- (bc-) plane indicate that one oxygen is on a fluoride site whereas the other one is on a neighbouring bromide site. The ^{17}O hf interaction parameters could only be determined for an orientation parallel to the c-axis (table 2). It is not clear which one should be assigned to the fluoride site and which one to the bromide site.

Although the chemical natures of the centres as being oxygen centres have been established from EPR, the exact site assignment cannot yet be made.

3.3. ENDOR measurements

ENDOR measurements were performed at temperatures of about 10 K. The EPR lines of the two new oxygen centres were superimposed by the very intense EPR lines of the two previously reported oxygen centres. The broad and very weak EPR signals of the two F centres ($F(Br^-)$ and $F(F^-)$ centres [5]) generated also were hardly detectable.

3.3.1. ENDOR measurements on the $(O^-_{Br})^*$ centre. The ENDOR spectrum measured on the EPR line of the $(O^-_{Br})^*$ centre for $\vec{B} \parallel \vec{c}$ (figure 3) shows many lines which do not all belong to the $(O^-_{Br})^*$ centre (see below). The g-values of table 1 indicate that for $\vec{B} \parallel \vec{c}$ the EPR line of

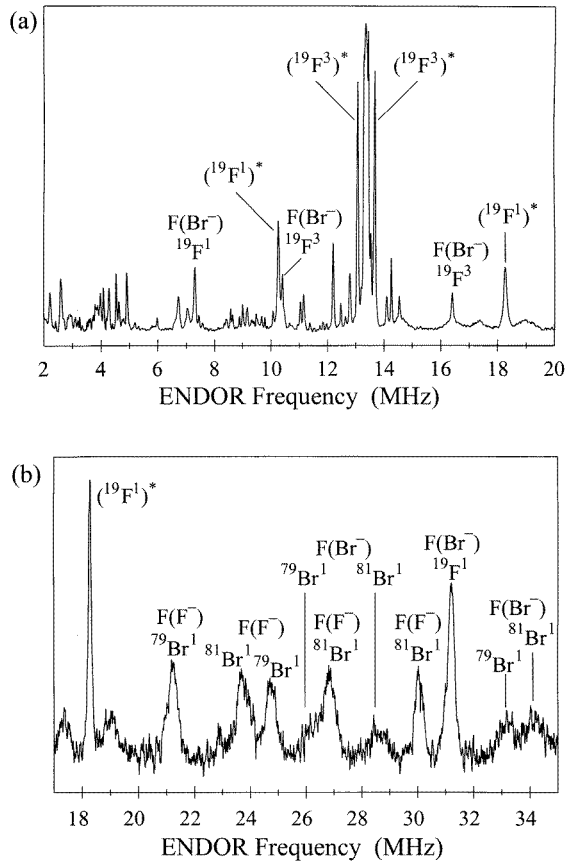

Figure 3. ENDOR spectrum measured at $B = 334.2$ mT and $T = 11$ K for $\vec{B} \parallel \vec{c}$ in BaFBr after x-irradiation at room temperature ($\nu = 9.339$ Hz). In figure 3(b) the scale is blown up by a factor of five compared to figure 3(a).

the centre superimposes the EPR lines of the F(Br$^-$) and of the F(F$^-$) centres. Therefore, the ENDOR spectrum can also contain lines of the F(Br$^-$) and of the F(F$^-$) centres, respectively. The two centres O_F^- [1, 2] and O_{Br}^- [4] are not seen in ENDOR lines at 10 K. They are only detectable below 8 K.

Most of the ENDOR lines are due to the F(Br$^-$) centre. Those of the first and third fluorine shell and the first bromine shell are labelled with F(Br$^-$) and $^{19}F^1$, $^{19}F^3$ or $^{79,81}Br^1$, respectively [5]. The lines of the two largest fluorine shf interactions of the $(O_{Br}^-)^*$ centre are from the first and third fluorine shell and are denoted by $(^{19}F^1)^*$ and $(^{19}F^3)^*$ in figure 3. Most of the ENDOR lines symmetrically placed around the intense line group around 13.4 MHz which coincides exactly with the Larmor frequency of ^{19}F ($B = 334.2$ mT) belong to the second or higher ^{19}F shells of the $(O_{Br}^-)^*$ centre or the F(Br$^-$) centre. The ^{19}F shf interactions of the F(F$^-$) centre are probably much smaller than those of the F(Br$^-$) centre as found in BaFCl [6]. Therefore, the F(F$^-$) ^{19}F ENDOR lines are probably also part of the line group around the ^{19}F Larmor frequency.

Because of the axial symmetry of the $(O_{Br}^-)^*$ centre there are two possible lattice sites and one interstitial site for the O$^-$ ion which all have four magnetically equivalent next bromine

neighbours for $\vec{B} \parallel \vec{c}$. The bromine shf interaction can be estimated from EPR line-width by using the formula [7]

$$(\Delta B_{1/2})^2 = \frac{8 \ln 2}{g^2 \mu_B^2} \sum_{i,l} N_l \xi_i A_{i,l}^2 \frac{I_{i,l}(I_{i,l}+1)}{3}. \quad (2)$$

$\Delta B_{1/2}$ is the half width (full width at half maximum = FWHM) of the EPR line, g the electronic g-factor, μ_B the Bohr magneton, N_l the number of nuclei in the lth shell, ξ_i the relative abundance of the ith isotope and $A_{i,l}$ the shf interaction parameter of the ith isotope in the lth shell.

$\Delta B_{1/2}$ of the $(O_{Br}^-)^*$ centre is $\leqslant 1.5$ mT for $\vec{B} \parallel \vec{c}$. According to equation (2) the upper limit of the bromine shf interaction is about 8 MHz. The corresponding ^{79,81}Br ENDOR lines would be below 10 MHz for $B = 334.2$ mT, i.e. some of the ENDOR lines between 2 and 10 MHz could be due to the first or higher bromine shells of the $(O_{Br}^-)^*$ centre. An exact analysis of the angular dependence of these bromine lines was not possible because of the superposition of too many lines. Moreover, the lines are too intense to be caused by shf interactions with Ba neighbours because of low abundance of magnetic Ba isotopes (natural abundance of ^{135}Ba with $I = 3/2$: 6.59%, of ^{137}Ba with $I = 3/2$: 11.2%).

The ENDOR lines between 20 and 35 MHz are all to due to bromine shf interactions. Some of them could be assigned to the first bromine shell of the $F(Br^-)$ centre, whereas the remaining ones could not be explained by bromine shells of the O_{Br}^- centre [4], the O_F^- centre [1, 2] or the $(O_{Br}^-)^*$ centre (see previous paragraph), respectively. Since the EPR line of the $F(F^-)$ centre has a $\Delta B_{1/2}$ of about 10 mT, the upper limit of its bromine shf interaction of the first shell is about 60 MHz. Thus the other ENDOR lines are to be assigned to the first bromine shell of the $F(F^-)$ centre labelled with $F(F^-)$ and $^{79,81}Br^1$ in figure 3(b). Unfortunately, the $F(F^-)$ centre concentration was not high enough to measure an angular dependence of these bromine lines necessary for a complete analysis. Table 3 shows only the shf and quadrupole parameters for $\vec{B} \parallel \vec{c}$.

Table 3. Shf and quadrupole parameters (first order perturbation theory) of the first bromine shell of the $F(F^-)$ centre in BaFBr for an orientation of the magnetic field parallel to the c-axis.

Centre	Shell	$A \parallel \vec{c}/h$	$Q \parallel \vec{c}/h$
$F(F^-)$	$^{81}Br^1$	∼46 MHz	∼1.0 MHz

The ENDOR angular dependence of figure 4 shows only lines of ^{19}F neighbours of the $(O_{Br}^-)^*$ centre. The bromine ENDOR lines were not intense enough to be detectable over a full angular dependence. The biggest shf interaction which we assign to the first fluorine shell is clearly visible and labelled with $^{19}F^1$. For a rotation of the magnetic field from the c-axis into the ab-plane and in the ab-plane we observed two pairs of two magnetically equivalent $^{19}F^1$ nuclei. The small splittings of the $^{19}F^1$ ENDOR lines in figure 4 are due to a slight misorientation of the crystal. For $\vec{B} \parallel \vec{c}$ or at an angle of 45° in the ab-plane, respectively, all four $^{19}F^1$ nuclei are magnetically equivalent. Such an angular dependence is only possible if the O^- in the $(O_{Br}^-)^*$ centre is placed on a bromide site.

The lines between 12.2 and 13.8 MHz are due to shf interactions with higher fluorine shells. We could analyse the next biggest fluorine interactions which are due to the third fluorine shell and labelled with $^{19}F^3$. The ^{19}F Larmor frequency and the line group symmetrically placed around it shift for a rotation of the magnetic field from parallel to the c-axis into the ab-plane to lower frequencies (figure 4(a)) since the position of the static magnetic field has to be varied according the EPR angular dependence of the $(O_{Br}^-)^*$ centre in this rotation plane (figure 1(a)).

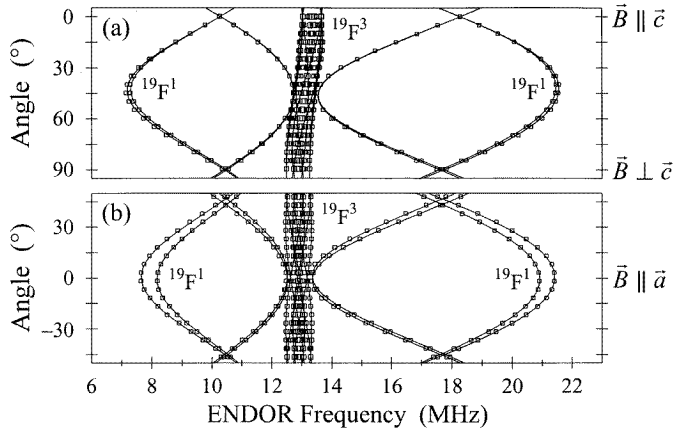

Figure 4. ENDOR angular dependence of the first and the third fluorine shell of the $(O^-_{Br})^*$ centre in BaFBr, measured at $T = 11$ K for a rotation of the magnetic field (a) from the c-axis into the ab-plane and (b) within the ab-plane. The open squares represent the experimental line positions; the solid lines are calculated by using the shf parameters of table 4.

This field correction was not necessary in the ab-plane where the angular dependence of the $(O^-_{Br})^*$ centre is isotropic.

The angular dependence of the first shell cannot be described with a symmetric shf tensor but with an asymmetric one as has been reported for the O^-_{Br} centre in BaFBr before [4]. The symmetry of the connection line between a $^{19}F^1$ neighbour and the $(O^-_{Br})^*$ centre is relevant. This connection line has monoclinic symmetry. Therefore, the shf tensor can be asymmetric and be determined by the parameters a, b and b', the angle ϑ between the z-axis of the tensor and the c-axis and an asymmetry parameter Δ as in equation (3) (for further details see [4, 8]).

$$\underline{\underline{A}} = \begin{bmatrix} A_{xx} & 0 & 0 \\ 0 & A_{yy} & 0 \\ 0 & 0 & A_{zz} \end{bmatrix} + \begin{bmatrix} 0 & 0 & 0 \\ 0 & 0 & A_{yz} \\ 0 & A_{zy} & 0 \end{bmatrix} = \begin{bmatrix} a-b+b' & 0 & 0 \\ 0 & a-b-b' & \Delta \\ 0 & -\Delta & a+2b \end{bmatrix}. \quad (3)$$

The parameters describing the $^{19}F^1$ angular dependence are collected in table 4.

Table 4. Shf parameters of the first and third fluorine shell of the $(O^-_{Br})^*$ centre, the first and second fluorine shell of the $(O_F–O_{Br})^{3-}$ centre and the first fluorine shell of the O^-_{Br} centre [4] in BaFBr.

Centre	Shell	a/h (MHz)	b/h (MHz)	b'/h (MHz)	Δ/h (MHz)	ϑ (°)	ψ (°)	ϕ (°)
$(O^-_{Br})^*$	$^{19}F^1$	8.09	7.27	0.02	−0.95	54	0	0
	$^{19}F^3$	−0.37	0.44	−0.08	—	71	25	−31
$(O_F–O_{Br})^{3-}$	$^{19}F^1$	0.11	1.58	0	—	78	0	−42
	$^{19}F^2$	1.37	2.10	~ -0.5	—	43	0	0
O^-_{Br}	$^{19}F^1$	19.03	11.16	−0.39	−3.35	53	0	0

Besides the first fluorine shell we could analyse the shf interaction of the third fluorine shell. The $^{19}F^3$–$(O^-_{Br})^*$ connection line has triclinic symmetry. Consequently, all nine tensor elements are independent from each other [8]. For the analysis of the $^{19}F^3$ shell we did not consider asymmetry parameters. The analysis yielded different signs for a and b. Since the anisotropic interaction parameter b is mainly determined by the classical point dipole–dipole

interaction [9] we assigned the negative sign to a (table 4). The orientation of each tensor is given by a set of Euler angles which is defined in figure 7.

ENDOR measurements on the ^{17}O hf lines of the $(O^-_{Br})^*$ centre for $\vec{B} \perp \vec{c}$ yielded a direct determination of the perpendicular component $A_\perp$ of the ^{17}O tensor and also the quadrupole interaction tensor $\underline{\underline{Q}}$. The quadrupole interaction constant q is related to the principal values of the axial quadrupole tensor by

$$Q_\perp = -q \qquad \text{and} \qquad Q_\parallel = 2q. \tag{4}$$

The hf interaction constants a and b and the quadrupole interaction constant q were found to have the same sign. The data for the ^{17}O interaction of the $(O^-_{Br})^*$ centre are listed in table 2. We chose for all the constants the positive sign.

3.3.2. ENDOR measurements on the $(O_F–O_{Br})^{3-}$ centre. The EPR measurements have already shown that the $(O_F–O_{Br})^{3-}$ centre is a complex-like oxygen defect which is orientated in a ac- (bc-) plane having an angle ϑ between the complex axis (g-tensor z-axis z_g) and the crystal c-axis of 54° (see figure 5).

The next fluorine neighbours of the $(O_F–O_{Br})^{3-}$ centre can be divided into two different shells having only one or two fluorine nuclei, respectively (see figure 5). The ENDOR angular dependence of figure 6 was measured for a rotation of the magnetic field from the c-axis into the ab-plane and in the ab-plane, respectively, where the position of the magnetic field has to be varied according to the EPR angular dependence of the $(O_F–O_{Br})^{3-}$ centre. In both rotation planes there are two pairs of two equivalent centre orientations, i.e. we could measure the ENDOR lines of two centre orientations simultaneously.

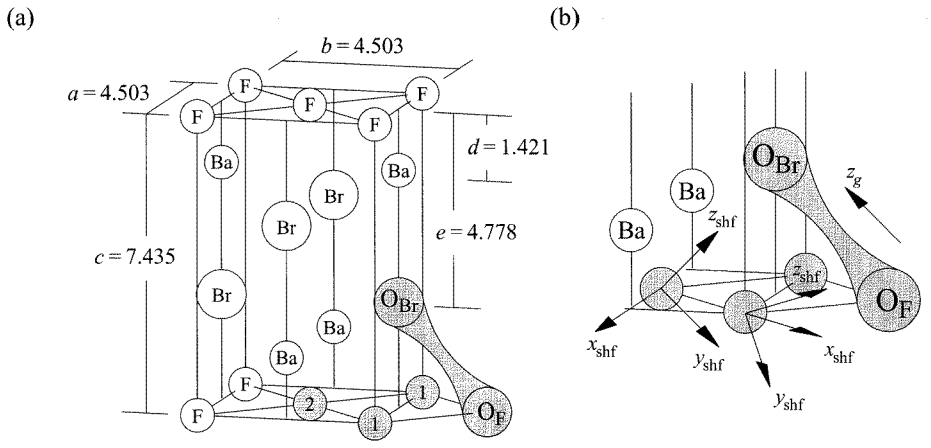

Figure 5. (a) Model of the $(O_F–O_{Br})^{3-}$ centre in BaFBr. The defect and its first (1) and second (2) fluorine shell is shaded. The separations between the ions are given for the unrelaxed lattice in Å [10]. (b) Principal axis system of the shf tensor of the first and second fluorine shell, respectively.

Figure 6 shows only lines of ^{19}F neighbours; ^{79,81}Br lines were not observed. In analogy to the $(O^-_{Br})^*$ centre the biggest ^{19}F shf interactions are assigned as due to the first and second fluorine shells (see figure 5). For the analysis of the first ^{19}F shell all nine tensor elements have to be determined since the $(O_F–O_{Br})^{3-}$–F^1 connection line has triclinic symmetry whereas the symmetry of the $(O_F–O_{Br})^{3-}$–F^2 connection line is monoclinic. ENDOR lines of higher fluorine shells symmetrically placed around the ^{19}F Larmor frequency could not be analysed because of the superposition of too many lines. The full angular dependence could be measured

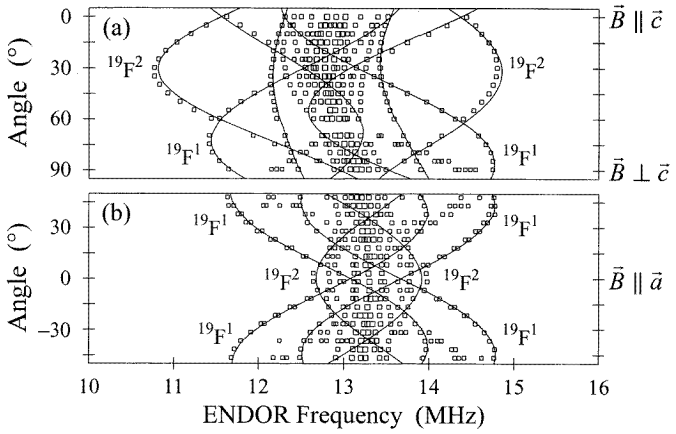

Figure 6. ENDOR angular dependence of the first and the second fluorine shell of the $(O_F–O_{Br})^{3-}$ centre in BaFBr, measured at $T = 11$ K for a rotation of the magnetic field (a) from the c-axis into the ab-plane and (b) within the ab-plane. The open squares represent the experimental line positions; the solid lines are calculated by using the shf parameters of table 4.

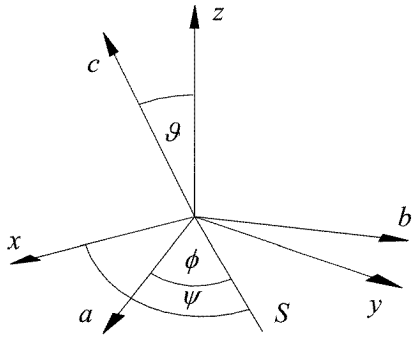

Figure 7. Definition of the Euler angles describing the tensor orientations. a, b and c are the crystal axes, whereas x, y and z are the principal axes of the tensor. In S the ab-plane cuts the xy-plane.

for the first shell in two rotation planes. The lines of the $^{19}F^2$ shell could be detected within the ab-plane only for a few degrees about the a-axis. The shf parameters are collected in table 4.

The EPR angular dependence has already indicated that the $(O_F–O_{Br})^{3-}$ centre is an oxygen molecule with one atom on a fluoride site and the other one on a neighbouring bromide site, both sharing one unpaired electron. This was confirmed by the ENDOR investigations. The z-axis of the shf tensor of the first fluorine shell is oriented almost exactly towards a fluoride site whereas that of the second fluorine shell is oriented towards the neighbouring bromide site (figure 5).

4. Discussion

The EPR and ENDOR analysis show that $(O^-_{Br})^*$ centre and the O^-_{Br} centre have the same symmetry and structure (O^- ion on a bromide site) but different shf interactions with the first fluorine shell. The much smaller $^{19}F^1$ shf interaction of the $(O^-_{Br})^*$ centre (see table 4) indicates that the distance between the $(O^-_{Br})^*$ centre and the first fluorine shell is bigger than that of the

O^-_{Br} centre. At least in one of the centres the position of the O^- must be influenced by a defect along the *c*-axis.

Before x-irradiation the oxygen ions of the $(O^-_{Br})^*$ centre and the O^-_{Br} centre, respectively, are incorporated as O^{2-} ions on bromide sites which requires the corresponding number of bromide or fluoride vacancies for charge compensation. Such a bromide vacancy could be the defect mentioned above. A fluoride vacancy cannot be responsible since the connection line between the oxygen centre and the defect must have axial symmetry along the *c*-axis. In principle it is also possible that the defect is a Ba^{2+} vacancy. However, for one Ba^{2+} vacancy in total there are three anion vacancies necessary for charge compensation which seems unlikely to happen. It is not possible to decide which of the two oxygen centres is 'distorted' and where a bromide vacancy may be located. It is also possible that both centres are 'distorted', having different distances between the O^- ion and the Br^- vacancy.

The structure of the $(O_F–O_{Br})^{3-}$ centre is analogous in a sense to that of the $V_K(Br^-_2)$ centre in BaFBr. However, the two nuclei are not residing on equivalent lattice sites. One oxygen nucleus is sitting on a fluoride site whereas the other one is on a bromide site. Since the separation of a fluoride and a neighbouring bromide site is 3.48 Å (see figure 5) but the internuclear distance of an O^{2-}_2 molecule in the range of 1.48–1.49 Å for crystalline compounds [11] it seems unlikely that the oxygen is incorporated in a molecular form. Before x-irradiation two adjacent diamagnetic O^{2-} ions may have been incorporated on adjacent F^- and Br^- lattice sites which then capture together one hole to form the paramagnetic $(O_F–O_{Br})^{3-}$ centre. It seems unlikely that these adjacent O^{2-} ions capture in total three holes to form a $(O_F–O_{Br})^-$ centre which would be paramagnetic as well.

In the case of a V_K centre the hole is equally distributed between the two halogens. Assuming a V_K-like structure of the $(O_F–O_{Br})^{3-}$ centre, the anisotropic part of the ^{17}O hf interaction can roughly be estimated using the data of the ^{81}Br hf interaction of the $V_K(Br^-_2)$ centre [12]. The anisotropic part of the ^{81}Br hf interaction is scaled by the ratio of the nuclear *g*-values and the $\langle r^{-3}\rangle$ expectation values [13].

$$b(^{17}O) \approx \left|\frac{g_n(^17O)}{g_n(^{81}Br)}\right| \left|\frac{\langle r^{-3}\rangle(2p, O^-)}{\langle r^{-3}\rangle(4p, Br^-)}\right| b(^{81}Br). \tag{5}$$

For an anisotropic part of the ^{81}Br hf interaction of about 340 MHz, equation (4) leads to an anisotropic part of the ^{17}O hf interaction of about 70 MHz. Since the two ^{17}O hf interaction values of the $(O_F–O_{Br})^{3-}$ centre are only slightly different we are using an average value of 120 MHz for $\vec{B} \parallel \vec{c}$ (table 2) corresponding to an hf interaction value for $\vec{B}$ parallel to the molecular axis of about 200 MHz. Since the anisotropic part of the ^{81}Br hf interaction of the $V_K(Br^-_2)$ centre is about 30% of the total hf interaction, this would in analogy lead to $b(^{17}O)$ of about 60 MHz in surprisingly good agreement with the calculated interaction of 70 MHz according to equation (4). Thus the suggestion that the $(O_F–O_{Br})^{3-}$ centre is of the V_K type seems justified. The hole is almost equally distributed between the two ions.

5. Conclusion

We have identified using EPR and ENDOR spectroscopy that the oxygen contamination of normally grown BaFBr single crystals give rise to four paramagnetic oxygen hole centres upon x-irradiation. The structure of which were identified to be O^-_F, two different O^-_{Br} and one molecular centre $(O_F–O_{Br})^{3-}$ or $(O_F–O_{Br})^-$; whether one or three holes were captured to form it cannot be decided from the experiment.

References

[1] Eachus R S, McDugle W G, Nuttall R H D, Olm M T, Koschnick F-K, Hangleiter Th and Spaeth J-M 1991 *J. Phys.: Condens. Matter* **3** 9327

[2] Eachus R S, McDugle W G, Nuttall R H D, Olm M T, Koschnick F-K, Hangleiter Th and Spaeth J-M 1991 *J. Phys.: Condens. Matter* **3** 9339

[3] Koschnick F-K, Spaeth J-M and Eachus R S 1992 *J. Phys.: Condens. Matter* **4** 3015

[4] Eachus R S, Nuttall R H D, Olm M T, McDugle W G, Koschnick F-K, Hangleiter Th and Spaeth J-M 1995 *Phys. Rev.* B **52** 3941

[5] Koschnick F-K, Hangleiter Th, Spaeth J-M and Eachus R S 1992 *J. Phys.: Condens. Matter* **4** 3001

[6] Bauer R U, Niklas J R and Spaeth J-M 1983 *Phys. Status Solidi* b **118** 557

[7] Seidel H and Wolf H C 1968 *Physics of Colour Centers* ed W B Fowler (New York: Academic) ch 8

[8] Alteheld P, Greulich-Weber S, Spaeth J-M, Weihrich H and Overhof H 1995 *Phys. Rev.* B **52** 4998

[9] Spaeth J-M, Niklas J R and Bartram R H 1992 *Structural Analysis of Point Defects in Solids (Springer Series in Solid-State Sciences 43)* (Berlin: Springer)

[10] Liebich B W and Nicollin D 1977 *Acta Crystallogr.* B **33** 2790

[11] Abrahams S C and Kalnajs J 1954 *Acta Crystallogr. Camb.* **7** 838

[12] Hangleiter Th, Koschnick F-K, Spaeth J-M, Nuttall R H D and Eachus R S 1990 *J. Phys.: Condens. Matter* **2** 6837

[13] Song K S and Williams R T 1996 *Self-Trapped Excitons (Springer Series in Solid State Sciences 105)* 2nd edn (Berlin: Springer)